minerals

MDPI

*Article*

# An Efficient and Economical Combination of Exploration Methods for Pb-Zn Polymetallic Skarn Deposits: A Case Study of the Periphery of Hetaoping Deposit, Yunnan Province, China

**Jingzi He [1,2], Tengfei Ge [2,3,*], Hongjie Tan [3], Xuzhao Huang [2], Shengqing Xiong [2,*], Zhengguo Fan [2] and Dalong Dai [4]**

[1] School of Geophysics and Information Technology, China University of Geosciences (Beijing), Beijing 100083, China; hejingzi@mail.cgs.gov.cn
[2] China Aero Geophysical Survey and Remote Sensing Center for Natural Resources, Beijing 100083, China; huangxuzhao@mail.cgs.gov.cn (X.H.); fanzhengguo@mail.cgs.gov.cn (Z.F.)
[3] School of Earth Science and Resources, China University of Geosciences (Beijing), Beijing 100083, China; thjthj1209@163.com
[4] Yunnan Institute of Geological Survey, Kunming 650216, China; alonggeo@126.com
* Correspondence: getengfei@mail.cgs.gov.cn (T.G.); xsqagrs@126.com (S.X.)

**Abstract:** The Hetaoping ore district in Baoshan City, Yunnan Province, is one of the major localities of Pb-Zn polymetallic skarn deposits in China, where geophysical and geochemical surveys play an important role in exploring Pb-Zn polymetallic mineral resources. Based on the exploration and prospecting carried out at the periphery of the Hetaoping Pb-Zn polymetallic deposit, this study proposed an aero-ground joint exploration method to determine the metallogenic model of distal skarns in the Hetaoping ore district, achieving ideal prospecting results. The steps of this method are as follows. First, the locations of ore-induced anomalies were determined using high-amplitude aeromagnetic anomalies. Then, the ore-induced anomalies were determined to be anomalies of Pb-Zn polymetallic deposits through geochemical surveys of soil samples and ground geophysical surveys. Based on these data, a quantitative analysis and metallogenic potential assessment of ore bodies and their surrounding rocks were conducted using the interactive 2.5D magnetic inversion. In addition, the 3D inversion of regional gravity data was also performed in order to determine the spatial location of the deep magma chamber. Accordingly, the metallogenic geological process in this area was analyzed by determining the spatial morphology of the deep magma chamber, and a prospecting model of the Pb-Zn polymetallic deposits was finally built. The results show that the aero-ground joint exploration method, which first conducts a rapid scanning survey using the aeromagnetic method and then locates, distinguishes, and assesses significant aeromagnetic anomalies by combining comprehensive verification means such as ground geophysical, geochemical, and geological surveys, is efficient and economical. This study will guide regional metallogenic research and the exploration and prospecting of Pb-Zn polymetallic deposits.

**Keywords:** Hetaoping; Pb-Zn polymetallic skarn deposit; aero-ground joint exploration method; verification of aeromagnetic anomalies; quantitative inversion

**Citation:** He, J.; Ge, T.; Tan, H.; Huang, X.; Xiong, S.; Fan, Z.; Dai, D. An Efficient and Economical Combination of Exploration Methods for Pb-Zn Polymetallic Skarn Deposits: A Case Study of the Periphery of Hetaoping Deposit, Yunnan Province, China. *Minerals* **2022**, *12*, 749. https://doi.org/10.3390/min12060749

Academic Editors: Kunfeng Qiu, Callum Hetherington, Maria Boni and Alireza Somarin

Received: 2 April 2022
Accepted: 9 June 2022
Published: 13 June 2022



## 1. Introduction

The Hetaoping ore district, located in the Southwestern Sanjiang region (Nujiang, Lancang, and Jinsha rivers in southeastern China) in the eastern Tethyan tectonic domain, is a major locality of Pb-Zn polymetallic skarn deposits in China [1–4]. Since the 1990s, several Pb-Zn polymetallic deposits have been discovered in this area, including

Jinchanghe [5,6], Hetaoping [7,8], Dachangwa [9], and Heiniuwa [10]. This ore district lies in a medium-high mountainous area with complex terrain and dense vegetation, making it difficult to carry out large-scale ground surveys. However, aeromagnetic surveys can greatly assist in geological prospecting, delineating concealed intrusions, and researching tectonic evolution in the above-mentioned areas [11–16]. From 2015 to 2017, the China Aero Geophysical Survey and Remote Sensing Center for Natural Resources (AGRS) undertook a high-precision aeromagnetic survey in the Tengchong–Yunxian area, Yunnan Province [17]. Previous researchers have carried out massive studies on the geological characteristics [18], ore-forming fluids [1,19], isotopic geochemistry [20,21], and timing of mineralization [22] in the Hetaoping ore district, while less attention has been paid to exploration methods of distal Pb-Zn polymetallic skarn deposits under the complex terrain conditions in this area. Therefore, based on previous results, we put forward an economical and efficient aero-ground joint exploration method. This study summarized the metallogenic process and the comprehensive prospecting models of Pb-Zn polymetallic deposits. Moreover, it provided important evidence for the existence of deep magma chambers under the Hetaoping ore district. All of these will provide effective guidance and new insights for future prospecting and exploration of the Hetaoping ore district. Taking the periphery of the Hetaoping Pb-Zn polymetallic deposit in Baoshan City, Yunnan Province, China, as a case study, we introduce in detail the application progress and the results of the aero-ground joint exploration method in prospecting Pb-Zn polymetallic skarn deposits.

## 2. Geological Setting

### *2.1. Regional Geological Setting*

The study area lies in the southeastern Lhasa block and the southeast side of the primary collision zone of the Eurasian and Indian plates [19,23,24] (Figure 1a). It is separated from the Simao block by the Changning–Menglian Paleo-Tethys suture zone in the east and is separated from the Tengchong block by the Gaoligong fault in the west [25,26] (Figure 1b). This area experienced the Late Paleozoic–Mesozoic Tethyan tectonic evolution and the superimposition and transformation induced by the Cenozoic continental collisional orogenesis, during which multiple episodes of large-scale mineralization occurred [20,22]. The Hetaoping ore district is located at the northern margin of the Baoshan block and near the Wayao fault in the middle part of the Lancangjiang deep fault. Owing to strong regional tectonic movements and complex geological evolution, the Hetaoping ore district enjoys rich and unique mineral resources and thus is an important part of the southwestern Sanjiang metallogenic belt.

Complete strata from the Pre-Sinian to the Quaternary have developed in the study area. Among them, the Paleozoic strata show the widest development, and their overlying Late Cambrian–Mesozoic sedimentary rocks mainly consist of neritic carbonate and clastic rocks. Moreover, the Lower Proterozoic–Triassic strata are dominated by marine sediments, the Jurassic–Cretaceous strata are mostly continental sediments, and the Paleogene–Quaternary strata comprise volcanos and sporadic intermountain basinal sediments [27]. The regional faults in the study area mainly have a nearly SN strike, such as the Lancangjiang, Nujiang, Kejie, and Wayaohe–Yunxian faults. Affected by the deep Lancangjiang fault, the tectonic fault lines in the study area mainly extend in the NW, NE, and SN directions (Figure 1b). Regional magmatic rocks were mainly formed by the eruption and intrusion of Permian basic magmas (e.g., the Woniusi basaltic complex with zircon U-Pb ages of 301–282 Ma [28,29]) and intrusion of Paleozoic–Cretaceous felsic magmas (e.g., the Gengma, Zhibenshan, and Caojian plutons [22,30]). Among them, granitic magmatism is closely related to the formation of Pb-Zn polymetallic skarn deposits in the Baoshan block [19,21,23,31–33].

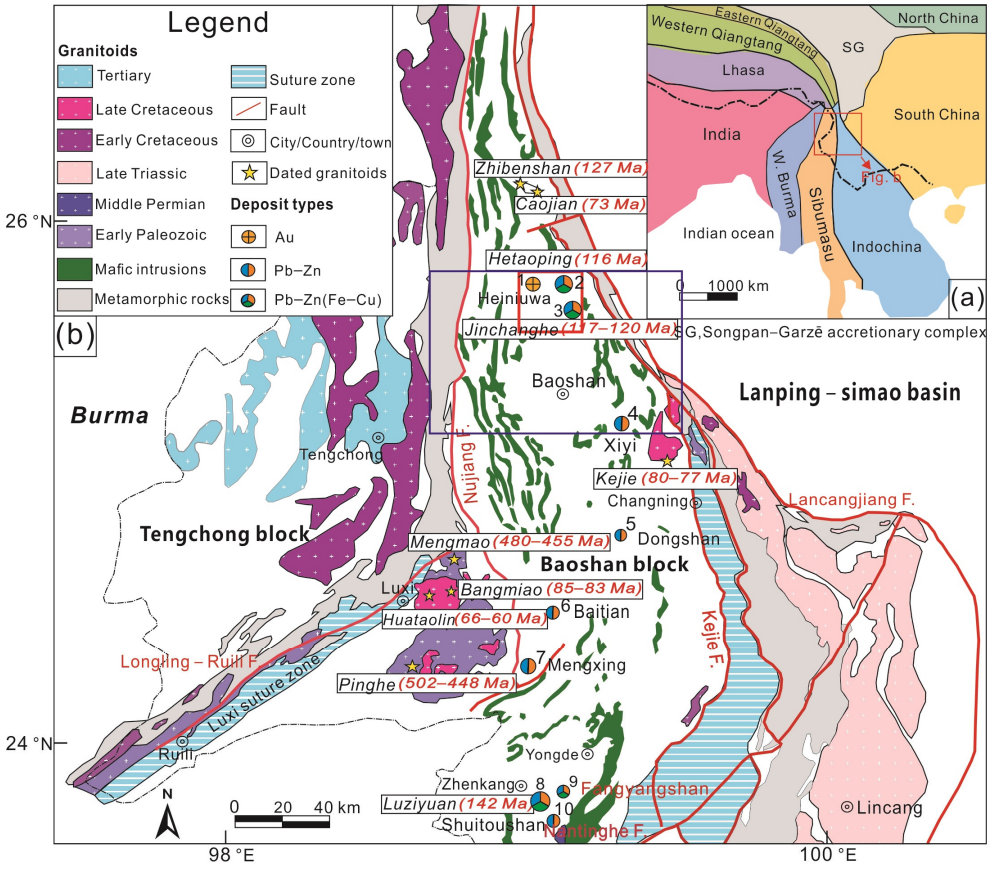


**Figure 1.** Sketch map showing the regional geology of the area under investigation. (**a**) Major continental blocks and suture zones in Southeast Asia (modified after [32]). (**b**) Simplified regional geologic map of the Baoshan block, showing the distribution of major structures, magmatic rocks, and ore deposits (modified after [19,28,31,33,34]).

### *2.2. Geological Setting of Deposits*

The Pb-Zn polymetallic deposits in the Baoshan block are skarn-type, which occur within carbonate strata and are controlled by faults. Deposits such as Hetaoping and Luziyuan are large-scale concealed Pb-Zn polymetallic deposits in the Baoshan block and have been explored and mined [5]. The Hetaoping ore district lies in the northern part of the Baoshan block (Figure 1b). The deposits in the Hetaoping ore district are controlled by two nearly SN strike first-order faults, namely, the Muguashu–Zhushijing fault (F21) and the Muguashu–Ashizai fault (F11). Moreover, the nearly SN strike secondary faults (F23–F30) sandwiched between the two first-order faults serve as the primary ore-transmitting and ore-hosting structures of the Hetaoping ore district. Strata exposed in the area mainly include the Hetaoping Formation, with the Shahechang and Baoshan formations locally exposed. The Hetaoping Formation is mainly composed of calcareous mudstones interbedded with siltstones and shales, marbleized limestones, and marls. The Shahechang Formation primarily includes marls, slates, shales, and siltstones. The Baoshan Formation consists of shales, sandstones, and limestones (Figure 2). The ore-hosting strata include carbonate rocks interbedded with clastic rocks in the Hetaoping, Shahechang, and Baoshan formations, and the ore-hosting surrounding rocks primarily include skarns. Moreover, some marbleized limestones, marls, and calcareous mudstones in the ore-hosting strata have undergone different degrees of skarnization and Pb-Zn mineralization [8,18,35]. The mineralization types mainly include skarn-type Pb-Zn(-Fe-Cu) polymetallic ore and skarn magnetite. Stratoid ore bodies occur intermittently along fault zones in the Hetaoping deposit, with the attitude roughly consistent with that of their surrounding

rocks. The main ore body has a length of 1.5 km along its strike, a thickness of approximately 8 m, a depth of approximately 200 m along its dip direction, and an average grade of Pb and Zn of 8.5%. Pb-Zn polymetallic deposits such as Dajinyan, Dachangwa, Hetaoping, Yizishan, Heiyanwa, and Jinchanghe have been discovered in the Hetaoping ore district [36].

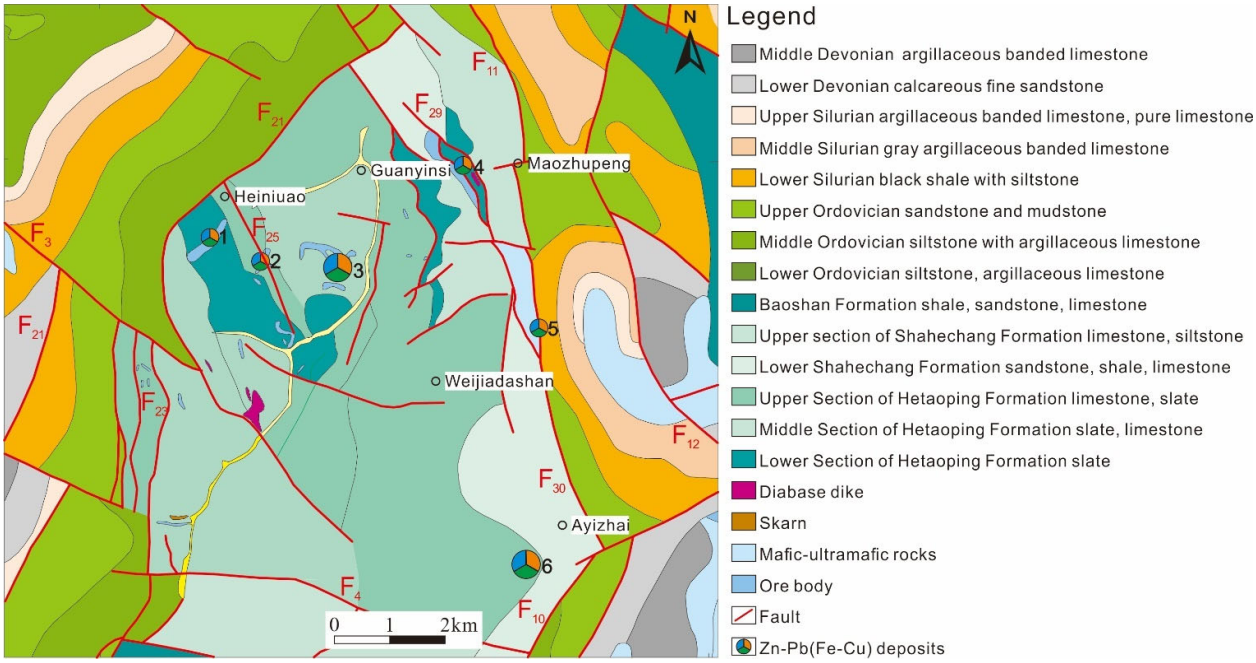


**Figure 2.** Geological map of the Hetaoping Pb-Zn deposit in Baoshan, Yunnan (modified after [37]). 1. Dajinyan Pb-Zn deposit; 2. Dachangao Pb-Zn deposit; 3. Hetaoping Pb-Zn deposit; 4. Yizishan Pb-Zn deposit; 5. Heiyanao Pb-Zn deposit; 6. Jinchanghe Pb-Zn deposit.

## 3. Data Acquisition and Processing

### *3.1. Aeromagnetic Survey*

The aeromagnetic data used in this study were derived from the project entitled "1:50,000 Aeromagnetic Survey of Tengchong-Yunxian Area, Yunnan Province" carried out by the AGRS from 2015 to 2017 [17]. In this project, the survey lines were EW-trending, with a line spacing of 500 m, and they were roughly perpendicular to the strike of major geological structures; the cross lines were deployed in the NS direction, with a line spacing of 10 km. This project was completed using a Squirrel helicopter (B-70DY) equipped with devices such as CS-3 optically pumped cesium vapor magnetometer sensors, DSC-1 data recording system and digital compensators, HD01 GPS, and BG3.0 radar altimeters. Moreover, the average flying height was 137 m, with a planar positioning accuracy better than 3 m and a total aeromagnetic survey accuracy of ±1.59 nanoTesla (nT).

The aeromagnetic data were preprocessed using the Oasis Montaj software developed by Geosoft and the GeoProbe software, Saline, KS, USA, independently developed by the AGRS. The data preprocessing mainly included coordinate projection transformation, the correction of the international geomagnetic reference field (2015 IGRF), diurnal variation, lag corrections, cross-line-based leveling, and microleveling. After data processing, the aeromagnetic data were gridded using the quadratic spline interpolation method, with a grid spacing of 100 m × 100 m (Figure 3a,b). To eliminate the impacts of oblique magnetization, reduction-to-the-pole (RTP) transformation was conducted using a frequency-domain algorithm for RTP at low magnetic latitudes (Figure 3c).

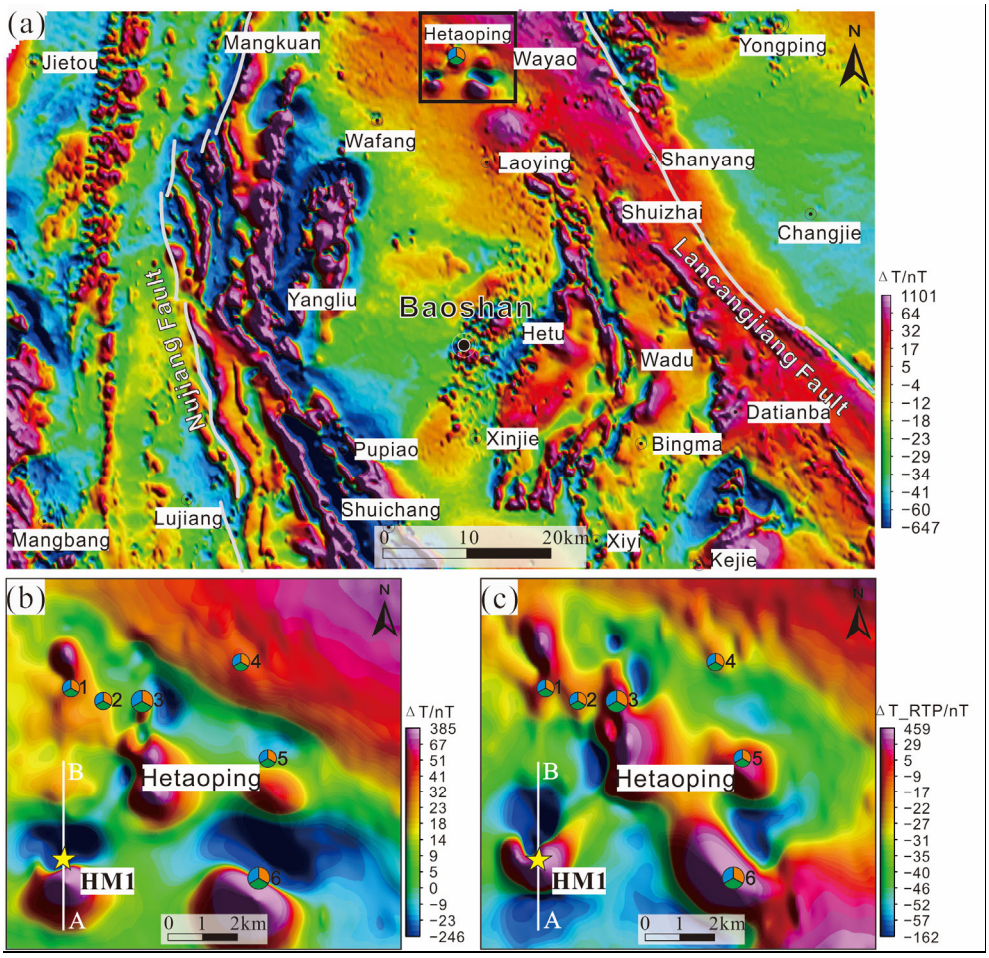


**Figure 3.** Aeromagnetic and RTP-transformed aeromagnetic shadow contour map of the study area. (**a**) Regional total magnetic intensity (TMI) shadow contour map. (**b**) TMI shadow contour map of Hetaoping ore district. (**c**) RTP-transformed aeromagnetic anomalies in Hetaoping ore district. Line AB is the location of the survey line, along which the ground magnetic, geological, and geochemical surveys were carried out. HM1 is the number of the aeromagnetic anomaly to be studied.

The aeromagnetic shadow contour map of the study area shows the characteristics of the regional magnetic fields (Figure 3a). The dominant aeromagnetic anomalies are NS-trending and almost parallel to the Nujiang and Lancangjiang faults. High-amplitude banded magnetic anomalies are distributed at the eastern edge of the Nujiang fault and the western edge of the Lancangjiang fault. This phenomenon is related to the felsic intrusions distributed along the faults and their contact zones. As a result, two significant aeromagnetic belts have formed in this area. Between those two aeromagnetic belts, low aeromagnetic anomalies are distributed in the Wafang–Baoshan–Shuichan area and correspond to the gravity lows in this area. There are several isolated aeromagnetic anomalies, including the studied aeromagnetic anomaly (No. HM1) lying in the Hetaoping ore district in Wayao Town, Baoshan City (Figure 3b). Additionally, HM1 is an aeromagnetic anomaly with high amplitude in a low background and shows high aeromagnetic gradients. To better align aeromagnetic anomalies with causative geological targets, RTP transformation was conducted (Figure 3c). As a result, the aeromagnetic anomalies correspond well to the six known deposits. Among the identified magnetic anomalies, HM1 is the most distinct one with no corresponding deposit.

### 3.2. Geological, Geochemical, and Magnetic Surveys

To investigate the aeromagnetic anomaly HM1, a ground magnetic survey, a geological survey, and a geochemical survey were carried out in the Hetaoping ore district. The survey line was numbered "Line AB" (Figure 3b,c), along which the spacing between adjacent measurement points was 40 m (Figure 4).

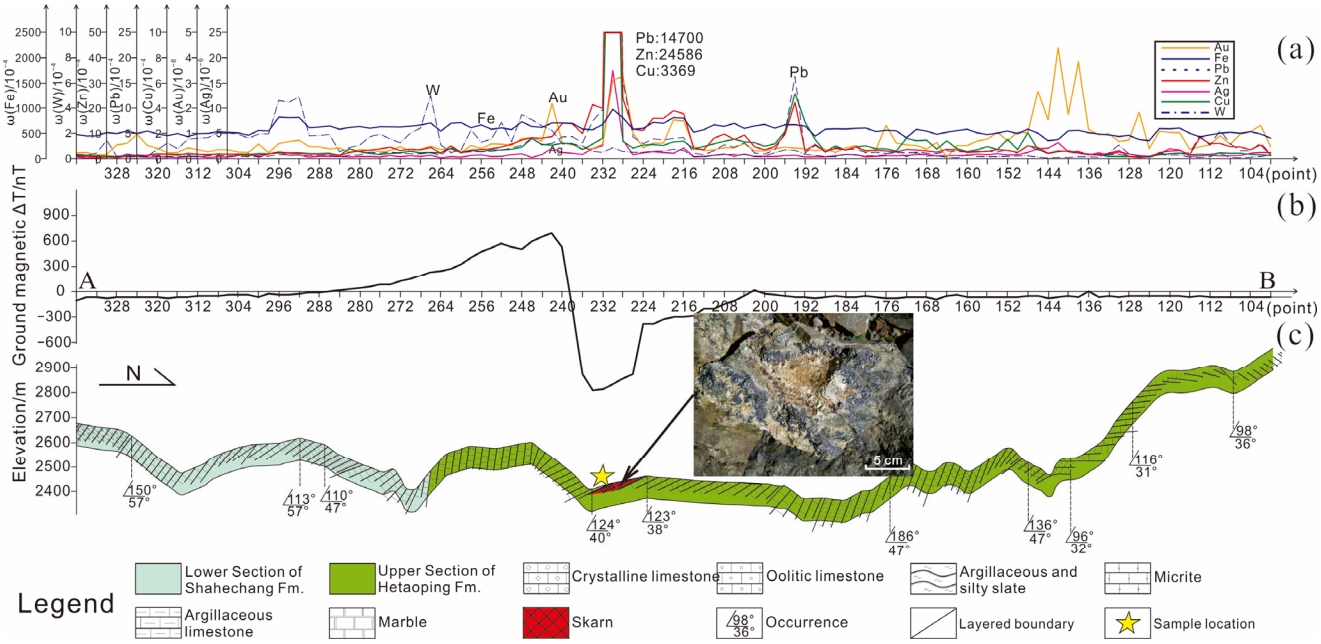


**Figure 4.** Integrated geological, geophysical, and geochemical survey sections along Line AB. (**a**) Geochemical survey section. (**b**) Ground magnetic survey section. (**c**) Geological survey section. The ore photo in Figure 4c shows the mineral distribution roughly.

A total of 119 soil samples (Figure 4a) and one rock sample (Table 1) were tested and analyzed at the Kunming Supervision and Inspection Center of Mineral Resources, Ministry of Land and Resources. The analyzed elements in geochemical samples included Cu, Pb, Zn, Au, Ag, W, Sn, Mo, Ni, total Fe (TFe), Hg, As, and Sb. The ground magnetic survey of the 119 measurement points was conducted using ENVI proton magnetometers manufactured by the Canadian Company Scintrex Ltd., Concord, ON, Canada, with an overall accuracy of 3.53 nT (Figure 4b). The field geological survey results are shown in Figure 4c.

**Table 1.** Rock sample geochemistry (No. H8).

| Au (ppm) | Ag (ppm) | Cu (wt%) | Pb (wt%) | Zn (wt%) | Ni (wt%) | Hg (ppm) |
|---|---|---|---|---|---|---|
| $0.69 \times 10^{-6}$ | $18.7 \times 10^{-6}$ | $0.42 \times 10^{-2}$ | $1.68 \times 10^{-2}$ | $3.64 \times 10^{-2}$ | $<0.002 \times 10^{-2}$ | $0.58 \times 10^{-6}$ |
| **TFe (wt%)** | **Mo (wt%)** | **Sn (wt%)** | **W (wt%)** | **As (ppm)** | **Sb (ppm)** | |
| $19.14 \times 10^{-2}$ | $<0.002 \times 10^{-2}$ | $<0.002 \times 10^{-2}$ | $0.034 \times 10^{-2}$ | $1278 \times 10^{-6}$ | $42.1 \times 10^{-6}$ | |

### 3.3. Magnetic Susceptibility Measurement of Rocks

Physical properties are the link between geology and geophysics, and the measurement, research, and analysis of the physical properties of rocks and ores can provide important constraints for the processing and interpretation of geophysical measurement results. A total of 131 samples were collected during the investigation of aeromagnetic anomalies performed in the Hetaoping ore district. The susceptibilities were measured using the KM-7 Susceptibility Meter produced by the Czech Republic (Table 2), and their remanent magnetization intensities (RMI) were measured by the second-position method [38] using proton magnetometers (Table 2).

**Table 2.** Statistics of magnetic parameters of rock samples collected from the Hetaoping ore district.

| Lithology | Sample Quantity | Susceptibility | | Remanent Magnetization Intensity *Jr*/($10^{-3}$A/m) | |
|---|---|---|---|---|---|
| | | Range | Average | Range | Average |
| Siltstones, silicified and pyritized fine sandstones | 13 | 0.2–266 | 221 | 0.1–231 | 100 |
| Mudstones, argillaceous siltstones | 15 | 0.2–271 | 62 | 0.1–236 | 8 |
| Limestones, finely crystalline limestones, marls | 17 | 239–339 | 91 | 5–34 | 13 |
| Calcareous and silty slates, marbleized limestones | 12 | 30–256 | 118 | 6–63 | 19 |
| Cataclasites, quartz veins | 4 | 63–312 | 199 | 20–108 | 57 |
| General mafic rocks | 15 | 20–113 | 72 | 5–111 | 22 |
| Diabases | 4 | 138–1090 | 477 | 11–869 | 249 |
| Pyritized magnetized mafic rocks | 4 | 7803–52,258 | 24,792 | 3512–24,349 | 18,046 |
| Ultramafic rocks | 3 | 61,325–442,103 | 21,7454 | 194,188–560,809 | 338,357 |
| Pb-Zn ores (bearing pyrite, limonite, and chalcopyrite) | 8 | 49–153 | 86 | 7–91 | 58 |
| Pb-Zn ores (bearing specularite and pyrite) | 7 | 3596–545 | 453 | 54–100 | 75 |
| Pb-Zn ores (bearing magnetite and pyrrhotite) | 6 | 3166–62,476 | 40,533 | 1539–136,516 | 61,055 |
| Pb-Zn ores in adits (bearing magnetite and pyrite) | 8 | 143,868–1,426,537 | 785,802 | 119,390–448,215 | 283,803 |
| Skarns | 9 | 66–16,381 | 3737 | 9–10,291 | 2073 |
| Granites | 6 | 15–1540 | 400 | 5–1310 | 178 |

According to the measurement results of magnetic parameters (Table 2), the Pb-Zn ores bearing magnetite and pyrrhotite have an average susceptibility of 40,533 × $10^{-5}$ SI and thus are considered ferromagnetic bodies, whereas the skarns have an average susceptibility of 3737 × $10^{-5}$ SI. Moreover, ultramafic rocks have high magnetic susceptibility. There are distinct magnetic differences between the surrounding rocks and magnetite-bearing Pb-Zn ores. Other rocks (limestones, sandstones, and slates) all have a small susceptibility and are almost nonmagnetic.

## 4. Results and Discussion

The success rate of prospecting can be significantly improved by comprehensively utilizing various exploration techniques. To determine the metallogenic model of distal skarn-type Pb-Zn polymetallic deposits in the Hetaoping area, this study proposed an aero-ground joint exploration method. Based on the prospecting carried out at the periphery of the Hetaoping Pb-Zn polymetallic deposit, the practicability and effects of the aero-ground joint exploration method were analyzed in detail as follows.

### *4.1. Determining Planar Locations of Ore Bodies through Magnetic, Geological, and Geochemical Surveys*

#### 4.1.1. Ground Magnetic Survey

The HM1 anomaly was distinctly present in the TMI shadow contour map (Figure 3b) and the ground magnetic survey results (Figure 4b), and no human-induced noise was observed near Line AB during the ground magnetic survey. The ΔT anomaly curve obtained in the 1:10,000 ground magnetic survey near Line AB was regular in shape, with an anomaly width of nearly 2000 m and greatly varying intensity (−1169–697 nT). The peak of high-amplitude ground magnetic anomalies lies about 227 m to the north of the peak of the high-amplitude aeromagnetic anomaly (HM1). The high-value area of RTP-transformed aeromagnetic anomalies is visible in the gray zone (1000–2700 m; Figure 5). The measurement results of magnetic susceptibility parameters (Table 2) show that the limestones and slates of the Cambrian Hetaoping and Shahechang formations in the Hetaoping ore district are

nonmagnetic or weakly magnetic. Therefore, it is considered that HM1 is induced by underground skarns and magnetite-bearing Pb-Zn ore bodies.

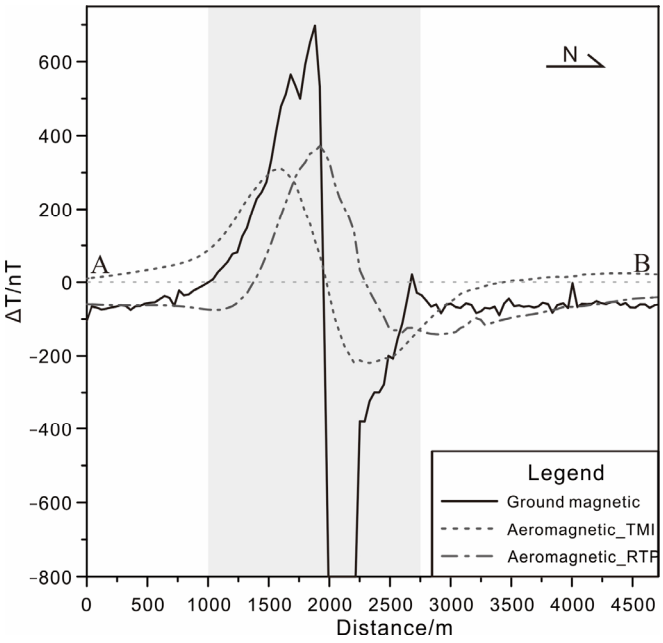


**Figure 5.** Aeromagnetic and ground magnetic anomaly curves of the section along Line AB. Aeromagnetic_TMI and Aeromagnetic_RTP anomaly curves were sampled from Figure 3b,c.

#### 4.1.2. Ground Geological Survey

The outcrops along Line AB mainly include the Cambrian Hetaoping and Shahechang formations consisting of argillaceous and silty slates, grayish limestones, and oolitic limestones (Figure 4c). Meanwhile, marbles and mineralized skarns are visible near ore bodies and alteration zones. The magnetic susceptibility measurements of the section along Line AB show that the lithologic strata are nonmagnetic, except for ferromagnetic grayish-black mineralized Pb-Zn(Fe-Cu) skarns and weakly magnetic grayish-black mineralized Pb-Zn and limonitized skarns. The characteristics of mineralized skarns are as follows.

Grayish-black mineralized Pb-Zn(Fe-Cu) skarns have a width of 12 m, strike of 110°∠45° (azimuth: 110°; dip: 45°), heteroblastic texture, and a massive structure. They are composed of garnet, pyroxene, idiocrase (vesuvianite), and epidote. In these rocks, chalcocite, galena, sphalerite, and magnetite form disseminations with veins and veinlets. Magnetite is distributed in the form of veinlets, stockworks, and clods.

Grayish-black mineralized Pb-Zn and limonitized skarns have a width of about 15 m, strike of 124°∠40°, heteroblastic texture, and a massive structure. They are composed of garnet, pyroxene, idiocrase, and epidote. In these rocks, disseminated Pb-Zn ores are unevenly distributed, and limonite is distributed in the form of veinlets along joints and fissures. Moreover, some actinolite is present as aggregates and in a radial form and with traces of magnetite within the ore body.

#### 4.1.3. Geochemical Survey of Soil Samples

Soil samples collected near Line AB were analyzed for geochemical element contents (Figure 4a). The results show that the Ag, Au, Cu, Pb, and Zn contents are anomalously high from Point 216 to Point 242, corresponding to the fractured zone of mineralized skarns in near-surface outcrops. Meanwhile, Cu, Pb, and Zn are locally enriched and correspond well to the locations of surveyed mineralized bodies and magnetic anomalies (Figure 4b,c). The contents of Ag, Au, Cu, Pb, and Zn in the soil are 0.78–17.5 g/t, 0.004–

0.032 g/t, 0.01–0.34%, 0.03–1.47%, and 0.087–2.46%, respectively. In addition, a geochemical sample (H8) was collected near Point 232. The geochemical analyses results of H8 show that the contents of Au, Ag, Pb, Zn, and TFe are 0.69 g/t, 18.7 g/t, 1.68%, 3.64%, and 19.14%, respectively (Table 1), indicating high contents of TFe, Pb, and Zn.

Overall, the analysis of aeromagnetic and geomagnetic anomalies suggests that HM1 is an ore-induced anomaly zone. The ground geological survey revealed mineralized Pb-Zn(-Fe-Cu) skarns at the location of HM1 near a fault. Moreover, HM1 corresponds well to the locations of anomalously high Cu, Pb, and Zn contents in the surface soil samples. Therefore, it can be inferred that the anomaly area HM1 in the Hetaoping ore district is mainly caused by underground magnetite-bearing Pb-Zn polymetallic ore bodies.

### *4.2. Determining the Spatial Locations of Ore Bodies through Inversion of Aeromagnetic Data*

To quantitatively calculate the occurrence space of underground concealed ore bodies, the 2.5D constrained inversion along Line AB was conducted using the Modelvision software based on the measured geomagnetic and geological data, as well as the data on the magnetic susceptibility parameters of rocks and ores (Figure 6). During the inversion, the surface morphology was considered. As the inversion results show, magnetic anomalies are mainly caused by veined skarns and magnetite-bearing Pb-Zn polymetallic ore bodies; the distribution of the skarns is controlled by faults, and there is a close spatio-temporal relation between the ore bodies and the skarns. The ore bodies are locally rich and occur in skarns in the form of steep layers. Their top has a burial depth of about 150 m, and they extend up to approximately 500 m. Moreover, their top corresponds to the center of the negative geomagnetic anomaly and the high-value RTP-transformed aeromagnetic anomaly of Line AB.

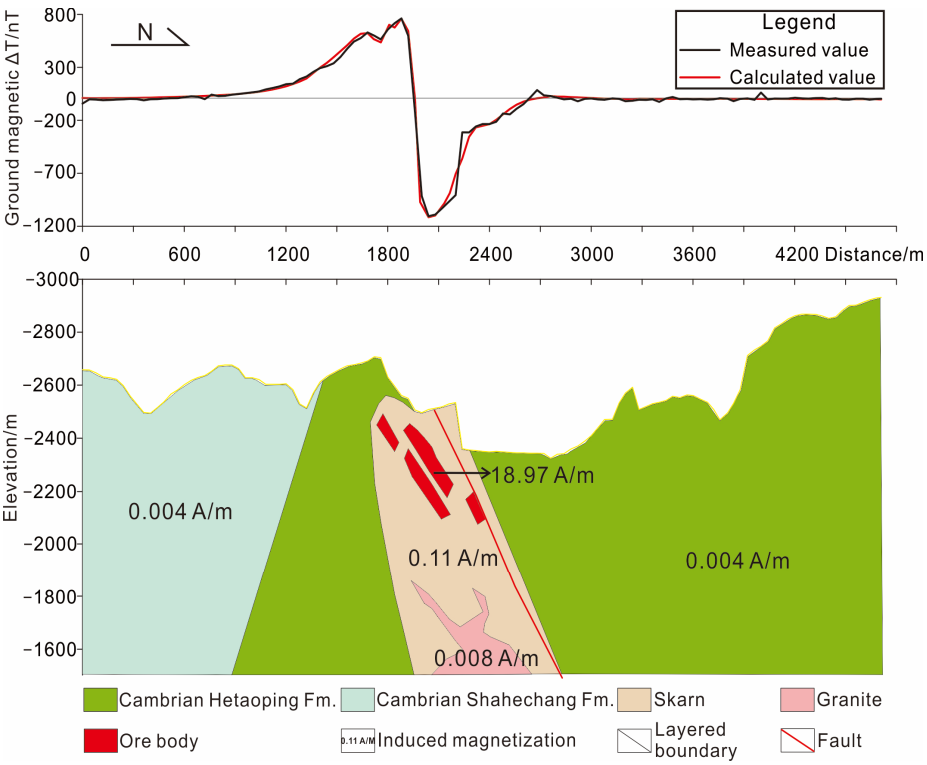


**Figure 6.** The 2.5D inversion results of the section of Line AB. $M_i = \kappa \times (T/\mu_0)$, where $M_i$ is induced magnetization, $\kappa$ is the magnetic susceptibility, and $\mu_0$ is permeability of vacuum and is set to a constant $1.256637 \times 10^3$ nT·m/A. Moreover, geomagnetic field intensity $T$ in the Hetaoping area is approximately 47,679 nT.

### *4.3. Determining Deep Intrusion Space through 3D Inversion of Regional Gravity Data*

The genesis of the Pb-Zn polymetallic deposits in the Hetaoping ore district is yet to be determined. Many skarn bodies controlled by faults have developed in this area. They tend to be associated with Pb-Zn polymetallic ore bodies. Given this, most researchers consider that the Pb-Zn polymetallic deposits in this area are skarn-type deposits related to concealed felsic intrusions [7,20,22,31,39]. However, large-scale felsic magmatic intrusions have not been revealed at a depth of 0–1 km in this area. Therefore, the existence of felsic magma chambers in deeper parts of the crust has become the key to the genetic analysis of the deposits. The 3D inversion of regional gravity data allowed for determining the spatial distribution of a low-density body, which is considered the concealed felsic magma chamber in deeper parts of the crust.

The gravity data used for the 3D inversion in this study originated from Bouguer gravity data with a grid spacing of 2 km × 2 km prepared in the project entitled "Potential Assessment and Integration of Nationwide Important Mineral Resources in China" (Figure 7). Based on the gravity inversion theory proposed by [40,41], we conducted the 3D inversion of the gravity data of the study area using the UBC-GIF software, UBC Geophysical Inversion Facility, Vancouver, BC, Canada. The grid used in this study was composed of cubes with a size of 500 m × 500 m × 500 m and contained 203, 189, and 69 cubes in the east, north, and vertical directions, respectively.

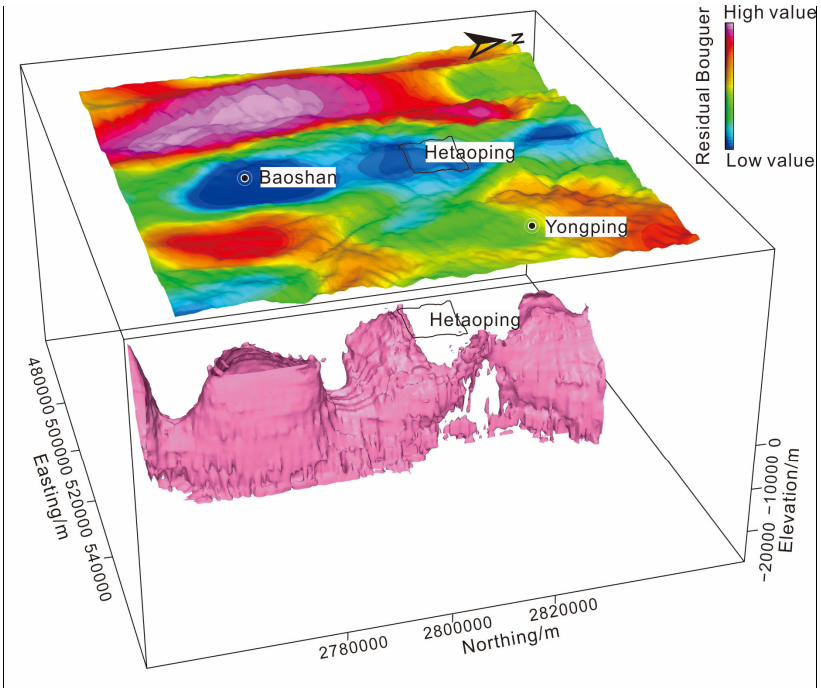


**Figure 7.** Spatial morphology of the deep magma chamber from the 3D inversion of gravity data. Residual Bouguer gravity anomalies were extracted using the square window moving average filtering method, and the side length of the sliding window was 30 km. The top colored shadow map shows the regional residual Bouguer gravity anomalies superimposed on the terrain, and the lower pink isosurfaces (density $\varrho = -0.032$ g/cm$^3$ [5,39]) are the inferred boundaries of deep concealed intrusions.

As shown by the inversion results, the deep concealed intrusions span across the central part of the study area and have an N-S strike, good continuity, and large extension. The concealed intrusions in the Baoshan area are large and extend deeply (depth: greater than 30 km). Some apophyses of them intrude into the shallow strata in the northwestern Hetaoping ore district. These deep intrusions may regionally connect with each other and form a giant magma chamber as a whole. In addition, as indicated by the zircon U-Pb dating and Hf isotopic analysis of the intrusions in the Baoshan area, the metallogenic

epoch of this area is consistent with the time of the Late Yanshanian magmatic activities and roughly corresponds to the closure time of the Meso-Tethys Ocean. Moreover, the Late Yanshanian magmatic activities formed in the extensional tectonic setting of the post-orogenic stage of the collisional orogenic belt [22]. This study provided important evidence for the existence of large magma chambers under the Hetaoping ore district, which supports the previous views that the hydrothermal source should be related to large and deep felsic intrusions. Based on these findings and combined with the regional tectonic and metallogenic background [42], the authors infer that numerous felsic magmatic rocks in the Baoshan block intruded during the closure of the Meso-Tethys Ocean due to the collision between the Tengchong and Baoshan blocks. In addition, it can be inferred that many Pb-Zn polymetallic deposits from the Hetaoping to Luziyuan areas in the Baoshan block may share the same magmatic-hydrothermal system, which is related to their polymetallic mineralization.

### *4.4. Metallogenic Geological Process and the Building of a Prospecting Model*

Well-developed metallogenic and prospecting models can effectively guide mineral exploration, thus promoting the development of the mineral industry. Therefore, this study summarized the metallogenic process of Pb-Zn polymetallic skarn deposit formation in the Hetaoping ore district and built a prospecting model (Figure 8).

#### 4.4.1. Analysis of the Metallogenic Process

As discussed above, the spatial morphology of the deep magma chamber was determined through the 3D inversion of regional gravity data. The authors believe that the Hetaoping Pb-Zn polymetallic deposit in the Hetaoping ore district is a distal skarn-type deposit controlled by the deep magmatic fluid system and is related to the Cretaceous tectono-magmatic activities (Figure 8). Many researchers have proposed and studied the distal skarn metallogenic system [43–51]. Fu et al. [5] inferred that concealed felsic intrusions exist in deep parts of the Hetaoping ore district based on geochemical anomalies, distinct gravity lows, and high-amplitude negative magnetic anomalies of the area. Based on isotopic tracer tests of Pb, S, H, O, C, and Si in Pb-Zn ore bodies in the Hetaoping ore district, Xue et al. [20] concluded that metallogenic hydrothermal solutions originated from the fractionation of deep-source magma or mantle-derived fluids and that the skarns in the Hetaoping ore district may be directly correlated to deep fluids or magmatic-hydrothermal solutions. In particular, the lead isotopic composition shows that the lead in the ore-forming fluids originates from a relatively consistent, stable lead source with orogenic belt characteristics, including a mixture of mantle- and crust-derived lead related to deep magmatism [20]. As indicated by the metallogenic, chronologic, and regional comparative study conducted by Tao et al. [22], the Hetaoping deposit is a magmatic skarn hydrothermal deposit related to the Late Yanshanian (116.1 ± 3.9 Ma) concealed granites. According to Chen et al. [8], the metallogenic fluids in Hetaoping are magmatic fluids, as indicated by the contents of trace elements in magnetite and pyrite. They also discovered that the temperature and oxygen fugacity of the ore-forming fluids and the degree of fluid–rock interaction jointly determined the temporal sequence and spatial zoning of magnetite and sulfide precipitation, resulting in the formation of the Hetaoping skarn-type Fe-Pb-Zn deposit. The aforementioned studies are consistent with the existence of the deep felsic magma chamber proposed in this paper. Based on the geological, geophysical, and geochemical analyses and the 3D inversion results of gravity data, the authors believe that the Pb-Zn polymetallic skarn deposits developing in the Hetaoping ore district experienced the following metallogenic process. Triggered by Cretaceous tectono-magmatic activities, the deep magmatic-hydrothermal solutions in the Baoshan block upwelled, providing sufficient thermal, water, and material sources for the formation of deposits in the Hetaoping ore district. The magmatic-hydrothermal solutions reached shallow favorable parts after migrating for a long distance along faults. Afterwards, they interacted with the surrounding rocks at a medium-low temperature, infiltrated, and

induced metasomatic replacement of surrounding rocks along the contact zones. As a result, a set of skarn mineral assemblages were formed and were then mixed with crustal fluids, leading to ore formation in shallow parts.

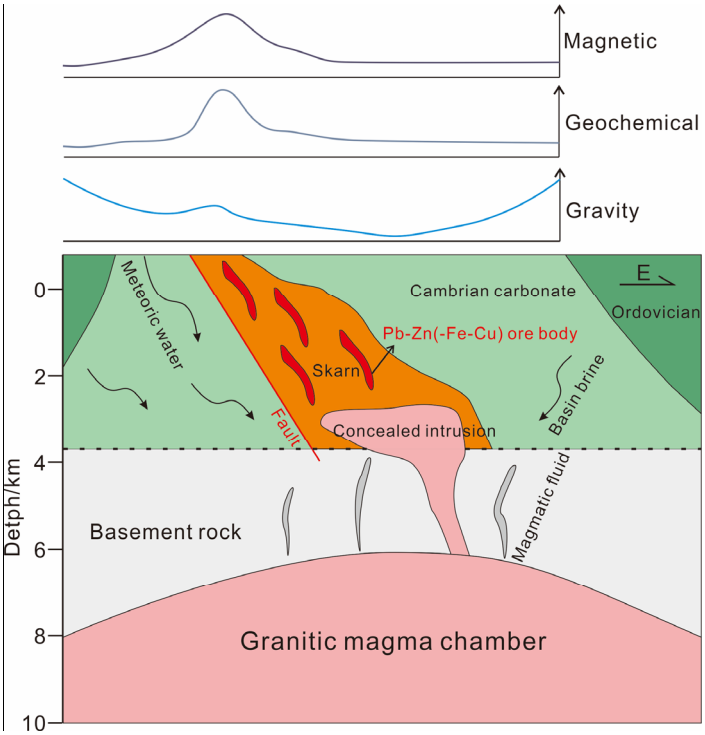


**Figure 8.** Metallogenic process and prospecting model.

4.4.2. Building of Prospecting Model

The ore types in the Hetaoping ore district mainly include distal skarn-type Pb-Zn polymetallic ores related to felsic intrusions. Many deposits of this type in this ore district show similar metallogenic characteristics. Therefore, it is feasible to establish unified prospecting indicators to serve the needs of exploration and prospecting. This study established a prospecting model of the Pb-Zn polymetallic deposits of this ore type from the geological, geophysical, and geochemical perspectives (Figure 8).

**In terms of geology:** Regional faults serve as the infiltration channels of magmatic-hydrothermal solutions and correspond to the locations of most skarn deposits. Small secondary faults determine the specific occurrence locations of skarns and are also the precipitation and accumulation sites of ore-bearing magmatic-hydrothermal solutions and ore-forming elements. The ore-bearing strata include the Upper Cambrian Hetaoping and Shahechang formations, which are primarily composed of limestones, dolomites, dolomitic limestones, and marbles, followed by slates and siltstones.

**In terms of geophysics:** Local low anomalies of regional gravity that reflect felsic intrusions exist. The surrounding rocks are weakly magnetic. By contrast, the skarn zones show high-amplitude magnetic anomalies, which occur as peaks on the whole. Magnetite is associated with polymetallic ores, and thus, the moderate- and high-amplitude anomalies in low magnetic fields serve as indirect indicators of this type of polymetallic ore.

**In terms of geochemistry:** The geochemical anomalies related to ore-forming geological bodies are usually distributed in a ring form around intrusions, and geochemically anomalous element associations in the soil samples are characterized by clear zoning. On the plane, Zn, Pb, Cu, Fe, Au, Ag, and W anomalies are distributed outward from the anomaly center in sequence. Along the studied profile, Cu, Pb, Zn, and Ag anomalies overlap, showing distinct concentration centers.

## 5. Conclusions

Based on the exploration at the periphery of the Hetaoping ore district, the authors consider that it is impractical to conduct exploration and prospecting in this area using only a geological prospecting model or simple geophysical or geochemical prospecting model or using all relevant technologies. Instead, the authors think that it is feasible to establish a comprehensive exploration positioning–rapid evaluation method using combined aero-ground exploration. The aero-ground joint exploration method for the Pb-Zn deposits at the periphery of the Hetaoping Pb-Zn polymetallic deposit can be summarized as follows: (1) Aeromagnetic anomaly zones and points were delineated through screening aeromagnetic anomalies via rapid scanning through aeromagnetic surveys. (2) The selected magnetic anomalies were determined to be ore-induced by analyzing the results of aeromagnetic anomalies. Then, the aeromagnetic anomalies were located, distinguished, and assessed using comprehensive verification means, such as high-precision ground geophysical, geochemical, and geological surveys. (3) It was revealed that the periphery of the Hetaoping Pb-Zn polymetallic deposit has great potential for the prospecting of other Pb-Zn polymetallic deposits through the quantitative 2.5D inversion based on human–computer interactions and 3D inversion.

The exploration at the periphery of the Hetaoping Pb-Zn polymetallic deposit in Baoshan verified that the aero-ground joint exploration method is both efficient and cost-effective for Pb-Zn polymetallic skarn deposits. Joint geophysical and geochemical exploration technology is the current trend in prospecting and exploration. The application of this technology provides a useful reference for increasing the peripheral reserves of deposits of the same genetic type in the Hetaoping ore district and may guide regional metallogenic research and ore prospecting.

Subject to time and funding constraints, this study has certain limitations. The authors will carry out electrical prospecting, drilling engineering verification, and more geochemical measurements of rock samples from the study area in the future.

**Author Contributions:** Conceptualization, J.H. and T.G.; methodology, J.H. and T.G.; software, J.H. and H.T.; validation, X.H. and D.D.; formal analysis, T.G.; investigation, J.H., T.G., X.H. and D.D.; resources, S.X. and Z.F.; data curation, J.H.; writing—original draft preparation, J.H., T.G., X.H. and D.D.; writing—review and editing, S.X. and Z.F.; visualization, J.H. and H.T.; supervision, X.H.; project administration, X.H.; funding acquisition, S.X. and Z.F. All authors have read and agreed to the published version of the manuscript.

**Funding:** This research was funded by the National Basic Research Program of China, grant number 2017YFC0602206, and the Projects of the China Geological Survey Bureau Program, grant numbers DD20190551 and DD20221640.

**Data Availability Statement:** Data sharing is not applicable to this article.

**Acknowledgments:** We would like to thank the Geological Survey of Yunnan Province for assistance with the work. We are also grateful to the anonymous reviewers, whose comments improved the quality of this manuscript.

**Conflicts of Interest:** The authors declare no conflict of interest.

## References

1. Yang, Y.L.; Ye, L.; Cheng, Z.T.; Bao, T. Origin of fluids in the Hetaoping Pb–Zn deposit, Baoshan-Narong-Dongzhi block metallogenic belt, Yunnan Province, SW China. *J. Asian Earth Sci.* **2013**, *73*, 362–371. https://doi.org/10.1016/j.jseaes.2013.04.036.
2. Deng, J.; Wang, Q.F.; Li, G.J. Tectonic evolution, superimposed orogeny, and composite metallogenic system in China. *Gondwana Res.* **2017**, *50*, 216–266. https://doi.org/10.1016/j.gr.2017.02.005.
3. Goldfarb, R.J.; Qiu, K.F.; Deng, J.; Chen, Y.J.; Yang L.Q. Orogenic gold deposits of China. *SEG Spec. Publ.* **2019**, *22*, 263–324. https://doi.org/10.5382/SP.22.08.
4. Qiu, K.F.; Goldfarb, R.J.; Deng, J.; Yu, H.C.; Gou, Z.Y.; Ding, Z.J.; Wang, Z.K.; Li, D.P. Gold deposits of the Jiaodong Peninsula, eastern China. *SEG Spec. Publ.* **2020**, *23*, 753–773. https://doi.org/10.5382/SP.23.35.
5. Fu, D.G.; Cui, Z.L.; Guan, D.R. The comprehensive ore-prospecting of Jinchanghe blind multimetallic deposit, Baoshan. *Yunnan Geol.* **2004**, *23*, 188–198. (In Chinese with English Abstract)

6. Wang, J.Y.; Yang, C.H.; Fu J.; Zhang, W.W.; Xie J.; Li J.B. Metallogenic models andprospecting criteria for the Jinchanghe Au–Cu polymetallic ore–concentration area in western Yunnan. *Geol. Explor.* **2021**, *57*, 0254–0268. https://doi.org/10.12134/j.dzykt.2021.02.002.
7. Chen, Y.Q.; Lu, Y.X.; Xia, Q.L.; Jiang, C.X.; Liu, H.G.; Lü, Z.C. Geochemical characteristics of the Hetaoping Pb- Zn deposit, Baoshan, Yunnan, and its genetic model and ore prospecting model pattern. *Geol. China* **2005**, *32*, 90–99. (In Chinese with English Abstract)
8. Chen, F.C.; Deng, J.; Wang, Q.F.; Huizenga, J.M.; Li, G.J.; Gu, Y.W. LA-ICP-MS trace element analysis of magnetite and pyrite from the Hetaoping Fe-Zn-Pb skarn deposit in Baoshan block, SW China: Implications for ore-forming processes. *Ore Geol. Rev.* **2020**, *117*, 103309. https://doi.org/10.1016/j.oregeorev.2020.103309.
9. Zhao, Z.X.; Wu, Z.Q. The metallogenetic rule and target seeking of Dachangao multimetal deposit in Baoshan. *Yunnan Geol.* **2008**, *27*, 338–343. (In Chinese with English Abstract)
10. Ma, Y.L.; Zou, R.R.; Wang, J.Y. Heiniuwa Au deposit of alteration rock type of fracture zone in Baoshan, Yunnan. *Yunnan Geol.* **2014**, *33*, 22–27. (In Chinese with English Abstract)
11. Shchukina, E.V.; Shchukin, V.S. Diamond Exploration Potential of the Northern East European Platform. *Minerals* **2018**, *8*, 189. https://doi.org/10.3390/min8050189.
12. Ge, T.F.; Qiu, L.; He, J.Z.; Fan, Z.G.; Huang, X.Z.; Xiong, S.Q. Aeromagnetic identification and modeling of mafic-ultramafic complexes in the Huangshan-Turaergen Ni-Cu metallogenic belt in NW China: Magmatic and metallogenic implications. *Ore Geol. Rev.* **2020**, *127*, 103849. https://doi.org/10.1016/j.oregeorev.2020.103849.
13. Zhang, J.; Zeng, Z.; Zhao, X.; Li, J.; Zhou, Y.; Gong, M. Deep Mineral Exploration of the Jinchuan Cu–Ni Sulfide Deposit Based on Aeromagnetic, Gravity, and CSAMT Methods. *Minerals* **2020**, *10*, 168. https://doi.org/10.3390/min10020168.
14. Lu, N.; Liao, G.; Xi, Y.; Zheng, H.; Ben, F.; Ding, Z.; Du, L. Application of Airborne Magnetic Survey in Deep Iron Ore Prospecting—A Case Study of Jinling Area in Shandong Province, China. *Minerals* **2021**, *11*, 1041. https://doi.org/10.3390/min11101041.
15. Ejiga, E.G.; Ismail, N.E.H.; Yusoff, I. Implementing Digital Edge Enhancers on Improved High-Resolution Aeromagnetic Signals for Structural-Depth Analysis around the Middle Benue Trough, Nigeria. *Minerals* **2021**, *11*, 1247. https://doi.org/10.3390/min11111247.
16. Kim, B.; Jeong, S.; Bang, E.; Shin, S.; Cho, S. Investigation of Iron Ore Mineral Distribution Using Aero-Magnetic Exploration Techniques: Case Study at Pocheon, Korea. *Minerals* **2021**, *11*, 665. https://doi.org/10.3390/min11070665.
17. He, J.Z.; Huang, X.Z.; Ge, T.F.; Fan, Z.G.; Dai, D.L.; Wang, S.X. Prospecting progress of aeromagnetic anomalies in the periphery of the Hetaoping Pb–Zn deposit, Baoshan, Yunnan Province. *Geophys. Geochem. Explor.* **2018**, *42*, 1201–1208. https://doi.org/10.11720/wtyht.2018.0033. (In Chinese with English Abstract)
18. Zhu, Y.Y.; Han, R.S.; Xue, C.D.; Lu, S.L.; Zou, H.J.; Yuan, Z.H. Geological character of the Hetaoping lead zinc deposit of Baoshan, Yunnan province. *Mineral Resour. Geol.* **2006**, *1*, 32–35. (In Chinese with English Abstract)
19. Chen, F.C.; Deng, J.; Shu, Q.H.; Li, G.J.; Cui, X.L.; Zhao, F.; Wang, Q.F. Geology, fluid inclusion and stable isotopes (O, S) of the Hetaoping distal skarn Zn–Pb deposit, northern Baoshan block, SW China. *Ore Geol. Rev.* **2017**, *90*, 913–927. https://doi.org/10.1016/j.oregeorev.2016.10.013.
20. Xue, C.D.; Han, R.S.; Yang, H.L.; Yang, Z.M.; Tian, S.H.; Liu, Y.Q.; Hao, B.W. Isotope geochemical evidence for ore-forming fluid resources in Hetaoping Pb–Zn deposit, Baoshan, northwestern Yunnan. *Miner. Depos.* **2008**, *7*, 243–252. (In Chinese with English Abstract)
21. Wang, Q.F.; Deng, J.; Li, C.S.; Li, G.J.; Yu, L.; Qiao, L. The boundary between the Simao and Yangtze blocks and their locations in Gondwana and Rodinia: Constraints from detrital and inherited zircons. *Gondwana Res.* **2014**, *26*, 438–448. https://doi.org/10.1016/j.gr.2013.10.002.
22. Tao, Y.; Hu, R.Z.; Zhu, F.L.; Ma, Y.S.; Ye, L.; Cheng, Z.T. Ore-forming age and the geodynamic background of the Hetaoping lead-zinc deposit in Baoshan, Yunnan. *Acta Petrol. Sin.* **2010**, *26*, 1760–1772. (In Chinese with English Abstract)
23. Chen, W.T.; Zhou, M.F.; Gao, J.F.; Hu, R. Geochemistry of magnetite from Proterozoic Fe-Cu deposits in the Kangdian metallogenic province, SW China. *Miner. Depos.* **2015**, *50*, 795–809. https://doi.org/10.1007/s00126-014-0575-7.
24. Chen, F.C.; Deng, J.; Wang, Q.F.; Li, G.J.; Shu, Q.H.; Yang, C.H.; Liu, J.Y.; Xu, R. The source and evolution of ore fluids in the Heiniuwa gold deposit, Baoshan block, Sanjiang region: Constraints from sulfide trace element, fluid inclusion and stable isotope studies. *Ore Geol. Rev.* **2018**, *95*, 725–745. https://doi.org/10.1016/j.oregeorev.2018.03.013.
25. Metcalfe, I. Tectonic framework and Phanerozoic evolution of Sundaland. *Gondwana Res.* **2011**, *19*, 3–21. https://doi.org/10.1016/j.gr.2010.02.016.
26. Li, G.J.; Wang, Q.F.; Huang, Y.H.; Chen, F.C.; Dong, P. Discovery of Hadean–Mesoarchean crustal materials in the northern Sibumasu block and its significance for Gondwana reconstruction. *Precambrian Res.* **2015**, *271*, 118–137. https://doi.org/10.1016/j.precamres.2015.10.003.
27. Xu, R.; Deng, M.G.; Li, W.C.; Lai, C.K.; Zaw, K.; Gao, Z.W.; Chen, Y.H.; Niu, C.H.; Liang G. Origin of the giant Luziyuan Zn-Pb-Fe(-Cu) distal skarn deposit, Baoshan block, SE Tibet: Constraints from Pb–Sr isotopes, calcite C–O isotopes, trace elements and Sm–Nd dating. *J. Asian Earth Sci.* **2021**, *205*, 104587. https://doi.org/10.1016/j.jseaes.2020.104587.
28. Liao, S.Y.; Wang, D.B.; Tang, Y.; Yin, F.G.; Cao, S.N.; Wang, L.Q.; Wang, B.D.; Sun, Z.M. Late Paleozoic Woniusi basaltic province from Sibumasu terrane: Implications for the breakup of eastern Gondwana's northern margin. *Geol. Soc. Am. Bull.* **2015**, *127*, 1313–1330. https://doi.org/10.1130/B31210.1.

29. Wang, Q.F.; Deng, J.; Li, G.J.; Liu, J.Y.; Li, C.S.; Ripley, E.M. Geochronological, Petrological, and Geochemical Studies of the Daxueshan Magmatic Ni-Cu Sulfide Deposit in the Tethyan Orogenic Belt, Southwest China. *Econ. Geol.* **2018**, *113*, 1307–1332. https://doi.org/10.5382/econgeo.2018.4593.
30. Yu, L.; Wang, Q.F.; Li, G.J.; Gao, L. Geochemistry, zircon U-Pb geochronology of granitic pegmatites from Caojian area in the northern Baoshan block, and their geological significance. *Acta Petrol. Sin.* **2015**, *31*, 3281–3296. (In Chinese with English Abstract)
31. Deng, J.; Wang, Q.F.; Li, G.J.; Li, C.S.; Wang, C.M. Tethys tectonic evolution and its bearing on the distribution of important mineral deposits in the Sanjiang region, SW China. *Gondwana Res.* **2014**, *26*, 419–437. https://doi.org/10.1016/j.gr.2013.08.002.
32. Metcalfe, I. Gondwana dispersion and Asian accretion: Tectonic and palaeogeographic evolution of eastern Tethys. *J. Asian Earth Sci.* **2013**, *66*, 1–33. https://doi.org/10.1016/j.jseaes.2012.12.020.
33. Deng, J.; Wang, Q.F.; Li, G.J.; Santosh, M. Cenozoic tectono-magmatic and metallogenic processes in the Sanjiang region, southwestern China. *Earth-Sci. Rev.* **2014**, *138*, 268–299. https://doi.org/10.1016/j.earscirev.2014.05.015.
34. Deng, X.Z.; Tao, Y.; Li, J.; Xiong, F. Isotope and fluid inclusion geochemistry of the Cangyuan Pb-Zn-Ag polymetallic deposit in Yunnan. SW China. *Ore Geol. Rev.* **2017**, *90*, 928–942. https://doi.org/10.1016/j.oregeorev.2017.05.034.
35. Wang, J.R.; Xue, C.D.; Huang, H.Y.; Jin, J.J. REE geochemical characteristics of Hetaoping Pb-Zn deposit, Baoshan county, western Yunnan province and its genetic implications. *Geoscience* **2014**, *28*, 721–730. (In Chinese with English Abstract)
36. Jiang, L.Y. The new cognition of metallogenesis characteristics of Hetaoping Pb-Zn multimetallic deposit in Baoshan. *Yunnan Geol.* **2011**, *30*, 38–41. (In Chinese with English Abstract)
37. Cui, Z.L.; Li, F.G.; Zhao, Z.X. *Geological Survey of Hetaoping Mining Area in Wayao Town, Baoshan City, Yunnan Province*; Fourth Geological Brigade of Yunnan Bureau of Geology and Mineral Resources: Baoshan, China, 1993; pp. 20–65. (In Chinese)
38. Guan, Z.N. *Geomagnetic Field and Magnetic Exploration*; Geological Publishing House: Beijing, China, 2005; pp. 77–83. (In Chinese)
39. Yang, X.W.; Guan, D.R. The comprehensive application of Geophys. Geochem. Explor. to Hetaoping ore deposit, Baoshan. *Yunnan Geol.* **2011**, *30*, 78–82. (In Chinese with English Abstract)
40. Li, Y.; Oldenburg D.W. 3-D inversion of magnetic data. *Geophysics*, **1996**, *61*, 394–408. https://doi.org/10.1190/1.1443968.
41. Li, Y.; Oldenburg D.W. 3-D inversion of gravity data. *Geophysics* **1998**, *63*, 109–119. https://doi.org/10.1190/1.1444302.
42. Goldfarb, R.J.; Mao, J.W.; Qiu, K.F.; Goryachev, N. The great Yanshanian metallogenic event of eastern Asia: Consequences from one hundred million years of plate margin geodynamics. *Gondwana Res*. **2021**, *100*, 223–250. https://doi.org/10.1016/j.gr.2021.02.020.
43. Einaudi, M.T.; Burt, D.M. Introduction; terminology, classification, and composition of skarn deposits. *Econ. Geol.* **1982**, *77*, 745–754. https://doi.org/10.2113/gsecongeo.77.4.745.
44. Meinert, L.D. Skarns and skarn deposits. *Geosci. Can.* **1992**, *19*, 145–162.
45. Meinert, L.D.; Dipple, G.M.; Nicolescu, S. World skarn deposits. In *Economic Geology 100th Anniversary Volume, 1905–2005*; Hedenquist, J.W., Thompson, J.F.H., Goldfarb, R.J., Richards, J.P., Eds.; Society of Economic Geologists Inc.: Littleton, CO, USA, 2005; pp. 299–336. https://doi.org/10.5382/AV100.11.
46. Vezzoni, S.; Dini, A.; Rocchi, S. Reverse telescoping in a distal skarn system (Campiglia Marittima, Italy). *Ore Geol. Rev.* **2016**, *77*, 176–193. https://doi.org/10.1016/j.oregeorev.2016.03.001.
47. Zhao, Y.M.; Dong, Y.G.; Li, D.X.; Bi, C.S. Geology, mineralogy, geochemistry, and zonation of the Bajiazi dolostone-hosted Zn–Pb–Ag skarn deposit, Liaoning Province, China. *Ore Geol. Rev.* **2003**, *23*, 153–182. https://doi.org/10.1016/S0169-1368(03)00034-9.
48. Xu, R.; Li, W.C.; Deng, M.G.; Zhou, J.X.; Ren, T.; Yu, H.J. Genesis of the superlarge Luziyuan Zn-Pb-Fe(-Cu) distal skarn deposit in western Yunnan (SW China): Insights from ore geology and C-H-O-S isotopes. *Ore Geol. Rev.* **2019**, *107*, 944–959. https://doi.org/10.1016/j.oregeorev.2019.03.015.
49. Xu, R.; Chen, W.; Deng, M.G.; Li, W.C.; Chen, F.C.; Lai, C.K.; Sha, J.Z.; Jia, Z.; Liu, W. Geology and C-O-S-Pb isotopes of the Fangyangshan Cu-Pb-Zn deposit in the Baoshan block (SW China) Implications for metal source and ore genesis. *Ore Geol. Rev.* **2021**, *132*, 103992. https://doi.org/10.1016/j.oregeorev.2021.103992.
50. Qiu, K.F.; Yu, H.C.; Deng, J.; McIntire, D.; Gou, Z.Y.; Geng, J.Z.; Chang, Z.S.; Zhu, R.; Li, K.N.; Goldfarb, R.J. The giant Zaozigou orogenic Au-Sb deposit in West Qinling, China: Magmatic or metamorphic origin?. *Miner. Deposita*, **2020**, *55*, 345–362. https://doi.org/10.1007/s00126-019-00937-w.
51. Qiu, K.F.; Yu, H.C.; Hetherington, C.; Huang, Y.Q.; Yang, T.; Deng, J. Tourmaline composition and boron isotope signature as a tracer of magmatic-hydrothermal processes. *Am. Mineral.* **2021**, *106*, 1033–1044. https://doi.org/10.2138/am-2020-7495.